Electronic Supplementary Information

A durable monolithic polymer foam for efficient solar steam generation

Qiaomei Chen[a], Zhiqiang Pei[b], Yanshuang Xu[a], Zhen Li[a], Yang Yang[a], Yen Wei[a]* and Yan Ji[a]*

[a]*MOE Key Laboratory of Bioorganic Phosphorus Chemistry & Chemical Biology, Department of Chemistry, Tsinghua University, Beijing 100084, China. E-mail: jiyan@mail.tsinghua.edu.cn, weiyen@tsinghua.edu.cn*
[b]*Simpson Querrey Institute for BioNanotechnology, Northwestern University, Chicago, Illinois 60611, USA*

1. Materials and methods

Synthesis of amino-capped aniline trimer (ACAT)
ACAT was synthesized by oxidative coupling of stoichiometric amount of bis (4-aminophenyl) amine sulfate hydrate and aniline with the oxidant ammonium persulfate in 1 M HCl solution, according to *Macromolecules* 1998, 31, 2702-2704.
Preparation of the NaCl template
According to *Tissue Eng.* 2002, 8, 43-52, NaCl powder was first thoroughly grounded and then sieved using a 300 meshes stainless steel sieve to screen the particles with sizes less than 50 μm. Then it was flatly paved into the mold with a size of 30 mm * 30 mm* 4 mm. The resulting NaCl template was subjected to 95% humidity for 4 h to achieve fusion of NaCl crystals prior to solution casting.
Preparation of the foam evaporator
Amino-capped aniline trimer (ACAT, 0.28814 g, 1.0 mmol) and paraformaldehyde (2.5 equiv, 0.075 g, 2.5 mmol) were weighed out into a round-bottom flask equipped with a magnetic stick. Then N-methylpyrrolidone was added (NMP, 4.0 mL). The mixture was reacted in an oil bath for 0.5 h at 50ºC with stirring. The above pre-polymerized solution was slowly casted into the above treated NaCl template until it was well-submerged. Then the whole reaction system was allowed to cure according to the following ramping procedure: 50ºC for 4 h, then 50°C - 200ºC for 1 h, and finally hold at 200ºC for 1 h in a heating jacket. The obtained material with NaCl template was carefully taken out from the mold and washed with deionized water for several times to remove the NaCl template. Finally, the porous polymer was dried in an oven at 80ºC for 24 h.

2. Characterization of ACAT

Chemical structure of ACAT was confirmed by liquid phase ^{1}H nuclear magnetic resonance (^{1}H NMR) spectroscopy, which was performed on a JEOL-ECX400 spectrometer in deuterated dimethyl sulfoxide (10 mg ml^{-1}) at 25ºC. Peaks appeared at 5.4 ppm are resulted from the terminal amine protons (–NH_2) of ACAT, and the rest characteristic peaks at the range of 7.0–6.5 ppm are in accordance with the aromatic proton of ACAT (Fig. S1). The fourier transform infrared spectroscopy (FTIR) of ACAT was conducted on a Perkin Elemer spectrum 100 at ambient temperature ranging from 4000 to 650 cm^{-1}. The characteristic absorption peaks appear at 3300 cm^{-1} and 3190 cm^{-1} are attributed to the terminal –NH_2. And the characteristic absorption peaks at 1598 cm^{-1} and 1499 cm^{-1} belong to the vibration of quinoid rings and benzenoid rings, respectively (Fig. S2).

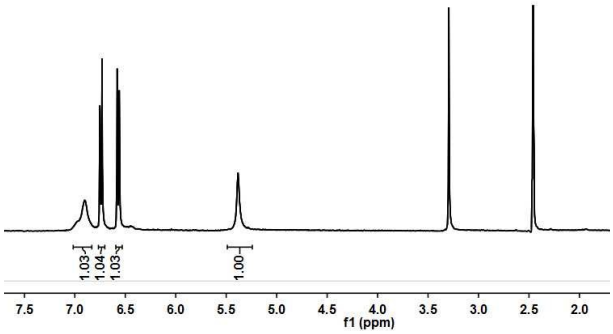

Fig. S1 [1]H nuclear magnetic resonance ([1]H NMR) spectroscopy of ACAT.

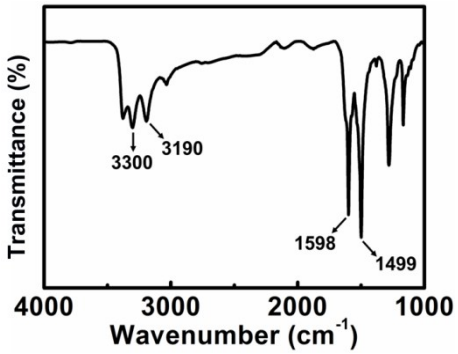

Fig. S2 The fourier transform infrared spectroscopy (FTIR) of ACAT.

3. Characterization of the foam evaporator

We confirmed the chemical structure of the foam by the fourier transform infrared spectroscopy (FTIR), X-ray photoelectron spectroscopy (XPS) and elemental analysis. As shown in Fig. S4, the characteristic absorption peaks located at 1598 cm^{-1} and 1499 cm^{-1} are attributed to the vibration of quinoid rings and benzenoid rings, respectively. The characteristic peaks of terminal amine (3300 cm^{-1} and 3190 cm^{-1}) disappeared, revealing that ACAT has been well-reacted with paraformaldehyde. New peaks appeared at 2850 cm^{-1} and 2920 cm^{-1}, which are resulted from the -CH2- of the hexatomic ring structure of the polymer. Unexpected OH stretching signal at 3380 cm^{-1} may be resulted from the side reactions previously reported. *Nat. Commun.* 2015, 6, 7417. The C 1s XPS spectrum of the polymer has a strong band of C-C/C=C species (284.8 eV, C of benzenoid rings) with a weak shoulder of C-N-C coordination (288.3 eV, C of hexatomic rings) (Fig. S5). The high-resolution N 1s spectrum (Fig. S6) reveals the typical C=N-C status of imine (399.8 eV) and no N-O_x groups (405.0 eV). The O 1s XPS spectrum (Fig. S7) consists of C-O groups (533.2 eV) and C=O groups (531.9 eV), which we suppose are mostly resulted from side reactions and the oxidation at high temperature, respectively. Elemental analysis (content %): N (16.71), C(70.53), H(4.63) and O(8.13), which is close to the ideal theoretical contents (N, C, H and O are 17.72%, 75.95%, 6.33% and 0%) with a small deviation due to side reactions and the oxidation.

Thermal properties of the evaporator were investigated using thermogravimetric analysis (TGA, TA-Q50) and differential scanning calorimetry (DSC, TA-Q2000). TGA of the evaporator was measured under both air and nitrogen atmospheres (Fig. S8) with a ramp rate of 20ºC min^{-1}, of which the corresponding onset of decomposition and 5% weight loss temperatures are 300ºC and 333ºC, respectively. The measurement procedure of DSC consisted of two scanning cycles ranging from 100ºC to 250ºC, of which both the heating and cooling rates were 10ºC min^{-1}, and the first scanning cycle was in order to eliminate the thermal history of the material. As shown in Fig. S9, the glass transition T_g is about 170ºC (the midpoint of the transition) upon heating.

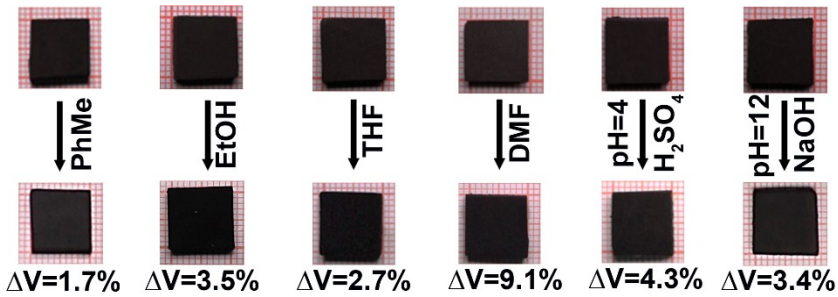

Fig. S3 Images of the evaporator before and after soaked in different solutions for 24 h.

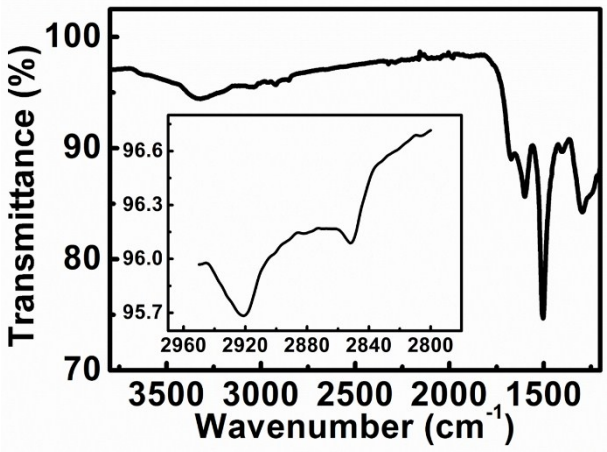

Fig. S4 The fourier transform infrared spectroscopy (FTIR) of the porous polymer photo-thermal evaporator.

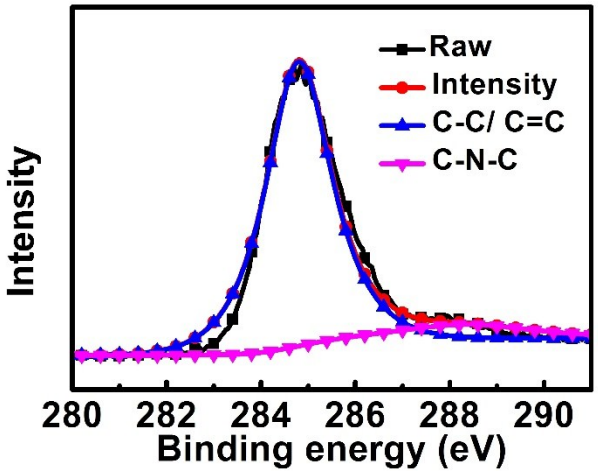

Fig. S5 The corresponding high-resolution C 1s peaks.

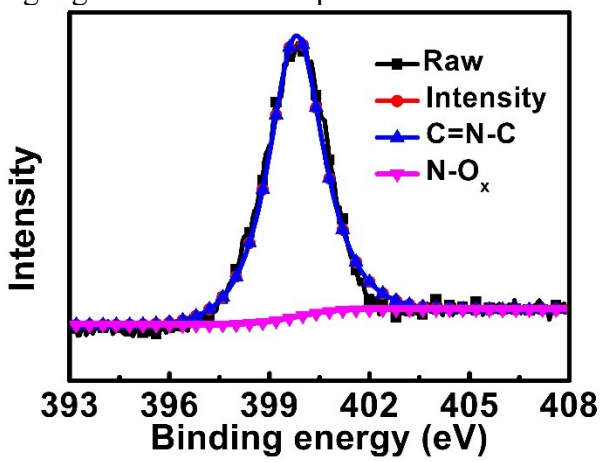

Fig. S6 The corresponding high-resolution N 1s peaks.

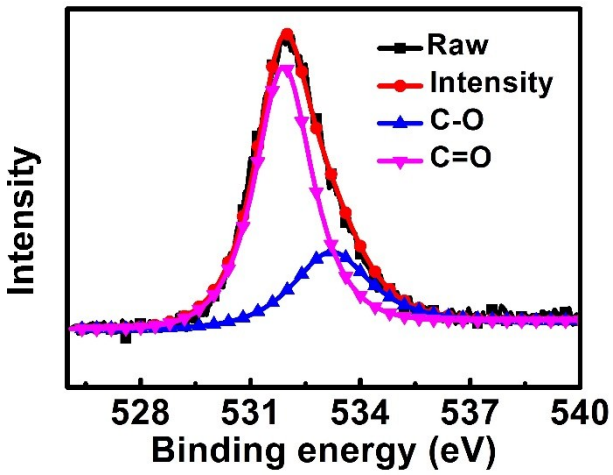

Fig. S7 The corresponding high-resolution O 1s peaks.

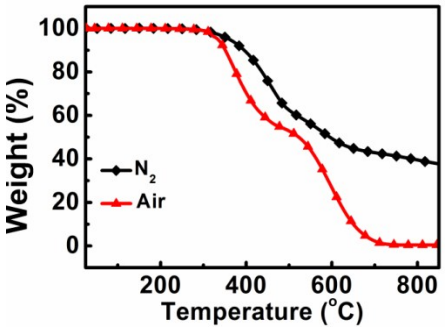

Fig. S8 TGA curves of the foam evaporator (heating rate: 20ºC min^{-1}).

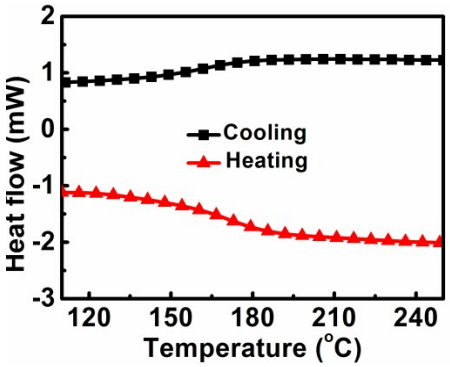

Fig. S9 DSC curve of both the heating and cooling procedures (rate of 10ºC min^{-1}).

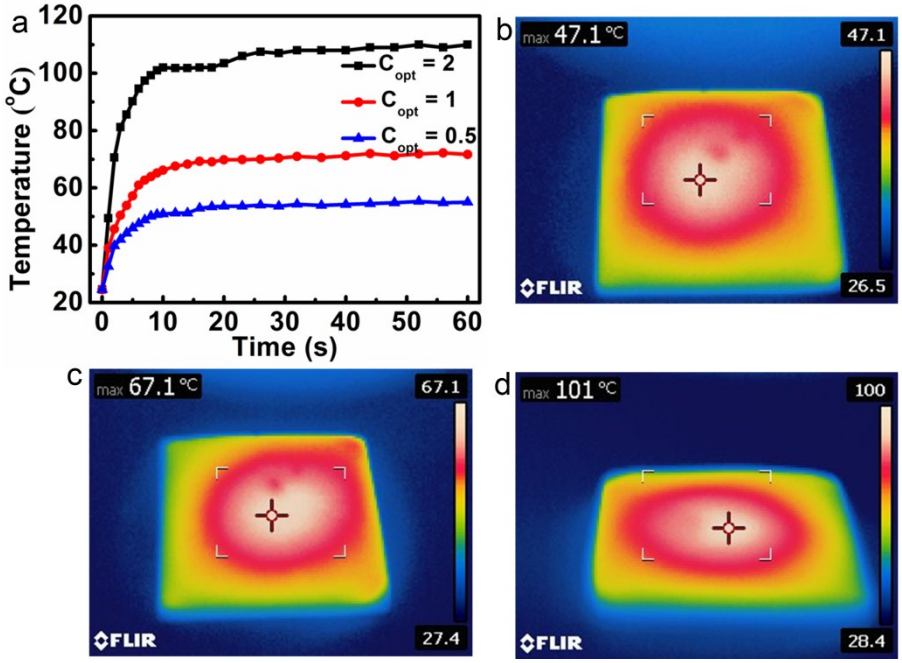

Fig. S10 Temperatures of the foam evaporator under different C_{opt}. (a) The surface temperatures of the foam evaporator under different solar intensities as functions of time. (b-d) The surface temperatures of the foam evaporator after 10 s solar illumination at C_{opt} = 0.5 (b), C_{opt} = 1 (c) and C_{opt} = 2 (d).

4. Steam generation experiments.

Energy conversion from solar illumination to thermal energy of the foam evaporator was tested by measuring the water evaporation rate using an experimental setup including a solar light illumination source, a scale, a test chamber and a data collection system. The test chamber consists of a cuboid quartz glass tube with inside length, width and height of 30 mm, 30 mm and 50 mm, respectively. To minimize the heat loss to the environment, we surrounded the glass tube with expanded polyethylene (EPE). The test chamber was placed on an electronic analytical scale (ME 204, Mettler Toledo) with a RS232C connecter to communicate with a computer. The solar light was simulated using a xenon arc lamp (Class ABA, CEL-S500, Ceaulight) with an air mass filter (AM 1.5G filter, Ceaulight), with the solar intensity calibrated with a VLSI standards incorporated PN 91150V Si reference cell (error: ≤1%). The weight and temperature changes were monitored in situ. The temperatures at the air-water interface (taken as the temperatures of steam) of the system were measured with an infrared thermal imager. The temperatures of water in the bottom of the glass tube were measured by placing the thermocouple (FLANK8855) adjacent to the bottom of the glass tube (about 40 mm from the air-water interface).

5. Estimation of energy conversion

The conversion efficiency η was calculated by the ratio between the harvested energy and the total solar energy according to the following formula (*Nat. Photonics* 2016, 10, 393–398),
$\eta = \dot{m}h_{LV}/C_{opt}P_0$
where $\dot{m}$ is the mass flux, h_{LV} denotes total latent enthalpy of the liquid-vapor phase change. P_0 refers to the optical intensity of one sun (1 kW m^{-2}) and $C_{opt}P_0$ represents the illumination intensity at air-water interface. The Mass fluxes under different solar intensity were obtained from the evaporation rate curves. We assume that the steam is generated at the balanced temperature, about 37ºC, 46ºC and 59ºC at C_{opt} = 0.5, C_{opt} = 1 and C_{opt} = 2, respectively (Fig.

S11). The harvested energy consists of the energy for heating the water (specific heat 4.2 J g^{-1} K^{-1}) and energy for liquid-vapor phase change at the balanced temperature. The corresponding heat of vaporization are calculated to be 2464.4 J g^{-1}, 2479.6 J g^{-1} and 2503.1 J g^{-1}, respectively. It should be noted that, the evaporation efficiency is lower at higher solar concentrations. Many factors may influence the evaporation rate, such as humidity, room temperature and steam diffusion rate. Moreover, the size, shape and thermal conductivity of the evaporation set-up will also influence the efficiency. As with our system, we think the most possible factors that can explain this question are the humidity and steam diffusion rate. During the evaporation process, the humidity around the device increases quickly but the steam generated can not diffuse quickly, which will suppress the evaporation rate. The effect will be more and more evident with the solar concentration increasing, leading to a decrease of efficiency with illumination increasing.

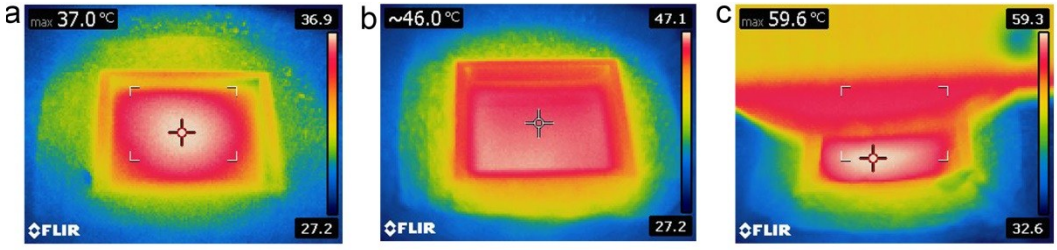

Fig. S11 The surface temperatures of the evaporator floated at the air-water interface after 15 min solar illumination at C_{opt} = 0.5 (a), C_{opt} = 1 (b) and C_{opt} = 2(c).

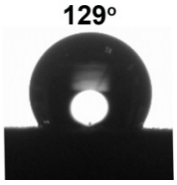

Fig. S12 Water wetting performance of the foam evaporator after 100 times water evaperation cycles.

6. Calculation of heat losses

The heat losses mainly include reflection of the polymer foam (about 5%), conduction to the underlying water, surface radiation and convective heat loss to the ambient. The test chamber parasitic loss is negligible for the excellent thermal insulation and the small lab-scale size of the test chamber. The surface radiation heat loss was calculated according to the Stefan-Boltzmann law:

$$q_r = A\varepsilon\sigma(T^4 - T_\infty^4)$$

where q_r is the heat flux (W m^{-2}), A is the surface area of the absorber facing the sun, ε the emittance of the absorbing surface (about 0.95 for our polymer foam) , σ the Stefan-Boltzmann constant (5.67×10^{-8} W $m^{-2}K^{-4}$, T the temperature of the irradiated polymer surface (about 46 ºC) and T_∞ the ambient temperature (about 28 ºC). Then the surface radiation heat loss is calculated to be 115 W m^{-2} (about 11.5% of the solar flux).

convective heat loss is calculated from the following formula:

$q_c = h(T - T_\infty)$

where q_c is the heat flux (W m^{-2}), h is the natural convection heat transfer coefficient (~5-10 W m^{-2} K^{-1}). This leads to a heat loss of 90-180 W m^{-2}, about 9-18% of the solar radiation.

As to the conduction to the underlying water, we estimate it to be 6% according to a very similar solar-thermal evaporation system (*Nat. Commun.*, 2014, **5**, 4449), where the conductive

heat loss is at most 6% at different solar concentrations (from 1 kW m^{-2} to 10 kW m^{-2}). Since the thermal conductivity of our polymer foam (0.057 W m^{-1} K^{-1}) is much lower than that of the above paper (0.93 W $m^{-1}K^{-1}$), the conductive heat loss of our system should be no more than 6%. The whole heat loss at 1 sun is calculated to be about 31.5%-40.5%.

According to the data disclosed in the papers with similar efficiency as ours (references in the main text), we can roughly calculate the heat losses as the following table 1, which are very close to ours.

Table 1 Heat losses of some similar papers with ours.

reference	η (experimental result)	ΔT (°C)	radiation heat loss	convective heat loss	optical heat loss	conduction heat loss (estimated)	heat loss
4	82%	25-41	9.60%	8-16%	8%	6%	31.6-39.6%
5	80%	17-39	12.80%	11-22%	6%	6%	35.8-46.8%
7	83%	22-44	13.60%	11-22%	5%	6%	35.6-46.6%

7. Analyzing of the condensed water vapor

The metal ion concentrations in the condensed water vapors from 3.5 wt% NaCl solution and 1 wt% mixed solution were studied by inductively coupled plasma spectroscopy (ICP–OES, TAS990). UV-vis spectra were utilized to determine the concentration of Rh 123 in the condensed water vapor. As shown in Fig. S13, the condensed water vapor from 100 ppm Rh 123 has the same adsorption spectrum with pure water, revealing that Rh 123 has been completely removed. PH of the collected condensed water vapor from the acid and base solutions were investigated with a pH meter (Mettler Toledo LE438), of which the pH were 6.94 and 7.25, respectively.

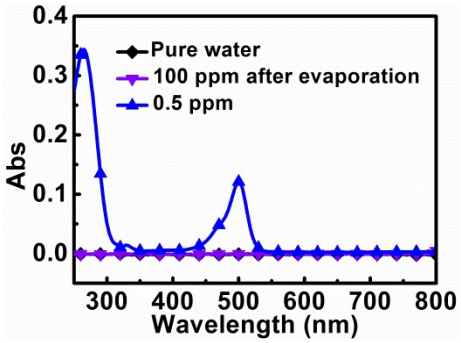

Fig. S13 UV-vis adsorption spectra of 0.5 ppm Rh 123, the condensed water vapor from 100 ppm Rh 123 and pure water.